

RESEARCH PAPER

Bio-directed Synthesis of Sm₂O₃ NPs by *Hibiscus Syriacus Ardens* flower extract as an effective catalyst in the preparation of benzimidazole derivatives

S. Marziyeh Kazemi¹, Asieh Yahyazadeh^{1*}, Navabeh Nami^{2*}

¹ Department of Chemistry, Faculty of Sciences, University of Guilan, Rasht, Iran

² Department of Chemistry, Qaemshahr Branch, Islamic Azad University, Qaemshahr, Iran

ARTICLE INFO

Article History:

Received 01 July 2021

Accepted 25 August 2021

Published 15 October 2021

Keywords:

Sm₂O₃ Nanoparticle

Benzimidazole-sugar

Rose of Sharon

Phytochemical synthesis

ABSTRACT

Double bloom purple Rose of Sharon, with the scientific name of *Hibiscus Syriacus Ardens* in the family of Malvaceae, was collected from Mazandaran, Iran in spring, dried in the shade, and powdered. The powdered flower material was extracted in ethanol (70% (V/V)). Samarium oxide nanoparticles (Sm₂O₃ NPs) were synthesized by using the Rose of Sharon flower extract. The morphology and structure of NPs were determined by FT-IR, X-ray diffraction (XRD), transmission electron microscopy (TEM), scanning electron microscopy (SEM), and energy dispersive spectra (EDS). Then, biosynthesized Sm₂O₃ NPs was used as a highly efficient catalyst for the synthesis of benzimidazole derivatives. These compounds were synthesized by the reaction of o-phenylenediamine and some sugars in the presence of Sm₂O₃ NPs (5 mol%) in ethanol 70%. The assigned structure was further established by CHN analyses, NMR, and FT-IR spectra. The catalyst was simply recovered, washed with ethanol, and reused 4 times without significant loss of activity.

How to cite this article

Marziyeh Kazemi S., Yahyazadeh A., Nami N. Bio-directed Synthesis of Sm₂O₃ NPs by *Hibiscus Syriacus Ardens* flower extract as an effective catalyst in the preparation of benzimidazole derivatives. *Nanochem Res*, 2021; 6(2):149-163. DOI: 10.22036/ncr.2021.02.003

INTRODUCTION

Rare earth oxide nanoparticles (REO NPs) such as samarium, yttrium, europium, and cerium, have gained much attention as important metal oxide NPs due to their various applications, including sensors, selective electrodes, and catalysis [1–3]. They have acquired considerable importance in organic synthesis because of their small size, large specific surface area, ease of handling, enhanced reaction rates, high selectivity, and simple workup [4–6]. They manifest good catalytic properties in several reactions including synthesis of ammonia and oxidative coupling of methane [7]. Owing to their intrinsic properties, samarium oxide

nanoparticles (Sm₂O₃ NPs) are one of the main rare earth oxide nanomaterials that are used in various fields such as nano-electronics, optics, infrared radiation-absorbing glass, solar cells, semiconductors, sensors, and catalysis [8–12].

On the other hand, heterocyclic compounds containing nitrogen such as benzimidazoles are very important chemical structures because of their biological and pharmacological activities such as anti-HIV, anti-bacterial, anti-histaminic, anti-cancer, anti-inflammatory, anti-oxidant, and anti-fungal [13–18]. They are also important in drug discovery [19, 20]. In addition, these chemical structures are good intermediates for the synthesis of some important organic compounds and drugs such as albendazole, omeprazole, mebendazole, etc

* Corresponding Author Email: navabehnami@yahoo.com
yahyazadehphd@yahoo.com

[21-23].

Scientists are very interested in the biosynthesis of nanomaterials using plants because this method focuses on the production of the desired product without producing harmful intermediate byproducts during the chemical reaction [24-33]. *Hibiscus Syriacus Ardens* belongs to the Malvaceae family, known as Rose of Sharon, which is a very common deciduous shrub that is native to Asia. Its name is derived from the blooms that some people find reminiscent of the prolific blooming pattern of shrub roses. In reality, this plant is a member of the Mallow family, and, viewed up close, its flowers resemble those of hollyhocks or hibiscus. This rangy shrub grows up to 12 feet tall and blooms vigorously from early summer and into the fall. Many flowers mean many seeds, and the Rose of Sharon is known to self-seed prodigiously, which can result in dozens, if not hundreds, of volunteer seedlings that spring up all around the garden and lawn. It prefers moist, well-drained soil but is tolerant of many growing conditions, including periods of drought and exposure to pollution, which makes it excellent for urban gardens [34, 35]. For the aforementioned reasons, we predict that samarium oxide nanoparticles can be helpful to increase the catalytic activity in the synthesis of benzimidazole derivatives. Therefore, in this paper we present a simple and inexpensive biosynthesis of Sm₂O₃ nanoparticles using double bloom purple Rose of Sharon extract in good yield and under mild reaction conditions. Sm₂O₃ NPs were used as an effective catalyst for the synthesis of some benzimidazole derivatives by the reaction of some sugars and *o*-phenylenediamine in ethanol 70%.

EXPERIMENTAL METHOD

Chemicals and Instrumentation

All chemicals and solvents were purchased from Merck and Aldrich. The production of nanocompounds was monitored by measuring the UV-Vis spectrophotometer (JENWAY 650), in the wavelength range of A200 to A800 nm and determined by powder X-ray diffraction (XRD) PW 3040/60 X'Pert PRO diffractometer system, using Cu K α radiation with ($\lambda = 1.5418 \text{ \AA}$) in the range of $2\theta = 20\text{--}80^\circ$ at room temperature. The morphology and sizes of NPs were evaluated using a scanning electron microscope (SEM) and transmission electron microscope (TEM, 150 kV, and Philips-CM 10) by Day Petronic Company-Iran. FT-IR measurements were recorded on a Shimadzu 8400s

spectrometer with KBr plates. The NMR spectra were recorded on Bruker XL 400 (400 MHz) instruments; mass-spectrometric measurements were made on an Agilent 6890 N Network GC system. The C, H, N analyses were performed by the microanalytical service of Day Petronic Company. Melting points were determined on an Electrothermal 9100 without further corrections.

Collection and preparation of purple Rose of Sharon flower extract

Purple Rose of Sharon was collected from Mazandaran, a province located in the north of Iran. The flower was first washed thoroughly in DI water, dried at room temperature for one week, and then ground in a blender before extraction.

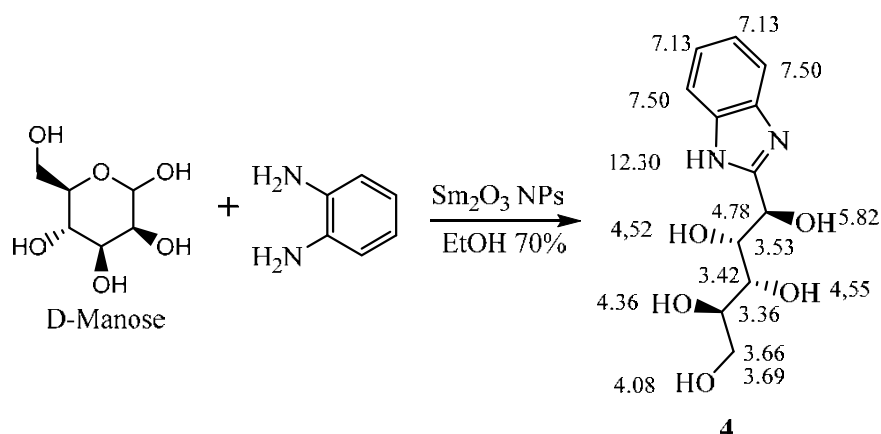
The powdered Rose of Sharon flower was weighed (500 g) in a beaker and percolated with ethanol 70% (V/V). This beaker was properly covered with aluminum foil and left for 72 hours. The solution was then filtered using a funnel filled in a filter paper and the extract was obtained. It was concentrated using a rotary evaporator and stored in the refrigerator at 4° C before use.

Preparation of Sm₂O₃ NPs

Rose of Sharon flower extract (0.5 g) was dispersed into 50 ml of ethanol: H₂O (1:1). The aqueous solution of Sm(NO₃)₃·6H₂O (0.3 g) in water (20 ml) was added dropwise into the reaction mixture through a dropping funnel by ultrasonication for 30 min and gently stirred at 60°C using a temperature-controlled magnetic stirrer for 2 h. After that, 0.02 M NaOH was added dropwise to the solution to achieve the pH of 10. The mixture was stirred for 24 extra hours. The completion of the reaction was monitored by UV-Vis spectra at 300-600 nm ($\lambda_{\text{max}} = 244, 324 \text{ nm}$). After the completion of the reaction, the precipitate was purified by several re-dispersions in deionized water and then centrifuged at 8000 rpm for 20 min and dried at 100 °C. The solid samples were then calcined at 500 °C for 4 h.

General procedure for the synthesis of benzimidazole derivatives

o-Phenylenediamine (1 mmol), sugar (1.5 mmol), and a catalytic amount of Sm₂O₃ NPs (5 mol%) were mixed and reacted in ethanol 70% (10 ml) under reflux conditions. The progress of the reaction was monitored by TLC using *n*-hexane: ethyl acetate (1:1) and detected by a UV lamp (254



Scheme 1. Synthesis of compound 4

& 366 nm). At the end of the reaction, the catalyst was separated by centrifugation, filtered, washed with ethanol and water, dried at 80 °C for 1h, and reused for the same reaction. The residue of the reaction mixture was evaporated, and the crude product was purified by recrystallization using ethanol and water. The products were determined by CHN analyses, NMR, and FT-IR spectra. The synthetic route for the same reaction has been presented in Scheme 1.

RESULTS & DISCUSSION

The present paper reports the results of the research aimed to verify the biosynthesis of the Sm₂O₃ NPs from purple Rose of Sharon flower extract as an effective catalyst in heterocyclic reactions. GC-Mass analyses of the Rose of Sharon flower were performed and various bioactive compounds were identified (Table1).

Optimization of different parameters

Some parameters like phytochemicals, phytochemical concentration, metal salt concentration, pH, and temperature can control the morphology, yield, stability, and rate of nanoparticle formation. The phytochemicals present in plant extracts of the reaction mixture have the potential to oxidize the metal ions in a much shorter time as opposed to other methods. Therefore, extracts are considered to be an excellent source for metal and metal oxide nanoparticle synthesis. The effects of the reaction conditions such as the ratio of plant extract and Sm(NO₃)₃, pH, reaction time, and reaction temperature were studied to maximize the yield of the nano compounds. The resulting

solutions of the reaction were monitored using a UV-Vis spectrophotometer. The influence of pH on the synthesis of Sm₂O₃ NPs was investigated at different values including 3.0, 5.0, 7.0, 8.0, 9.0, 10, and 11 (pH of Rose of Sharon flower extract solution was about 3.0). The reaction completion time was studied by monitoring the absorption spectra of nano compounds formed in the reaction media at different time durations (10 min to 48 h). Different ratios of plant extract and samarium nitrate solution were investigated (1:1, 1:2, 1:3, and 1:4) to find the maximum production of nanopowders. The reaction temperature was set at 25°C, 45°C, 65°C, and 85°C using the water bath for its optimization. The optimized condition of the reaction was obtained at room temperature in pH=10 after 24h with the ratio of 1:1 corresponding to the plant extract and samarium nitrate solution.

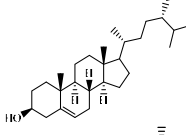
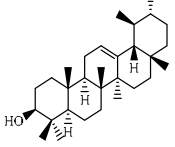
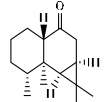
UV-Vis Studies

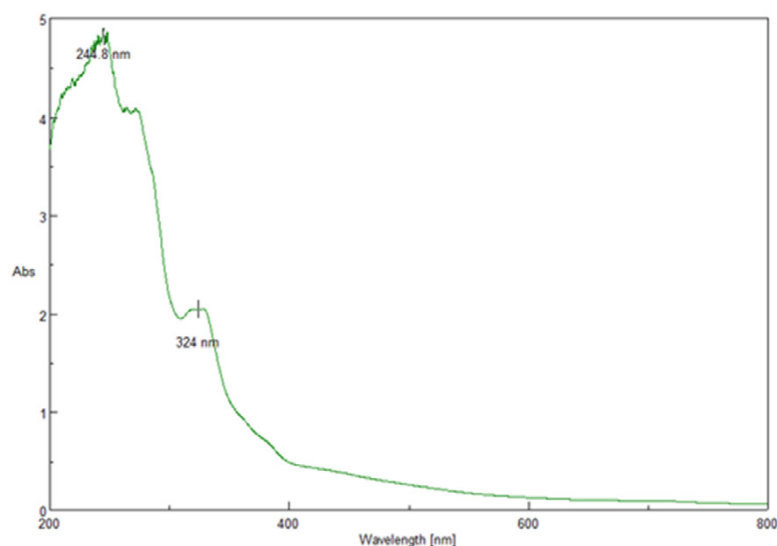
The completion of the reaction between Rose of Sharon flower extract, and samarium nitrate Sm(NO₃)₃ was monitored and optimized by taking the absorption spectrum in UV-Vis spectrophotometer at different reaction conditions. As the Rose of Sharon flower extract was added to the aqueous samarium nitrate solution, the color of the solution changed to colloidal dark brown with Sm₂O₃ colloids formation. The UV-Vis spectra were recorded after 10 min, 20 min, 60 min, 16 h, and 24 h at different temperatures (25°C, 45°C, 60°C, and 90°C) from the initiation of the reaction at the wavelength of 200-800 nm. The UV-Vis absorption spectra of biosynthesized Sm₂O₃ hybrid showed λ maxes at 244 and 324 nm (Fig. 1). The

Table 1. Phytochemicals of purple Rose of Sharon flower extract by GC-MS

| Entry | Name of the Compound | Molecular Formula (MF) | RT/Peak area % | Structure |
|-------|---|--|---------------------------|-----------|
| 1 | 1-Decyne | C ₁₀ H ₁₈ | 7.02/0.78 | |
| 2 | 2,3-Dihydro-3,5-dihydroxy-6-methyl-4H-pyran-4-one | C ₆ H ₈ O ₄ | 9.03/1.98 | |
| 3 | cytidine | C ₉ H ₁₃ N ₃ O ₅ | 13.39/5.70 | |
| 4 | Hexadecanoic acid | C ₁₆ H ₃₂ O ₂ | 19.39/14.93 | |
| 5 | Hexadecanoic acid, ethyl ester | C ₁₈ H ₃₆ O ₂ | 19.89/1.74 | |
| 6 | 9,12-Octadecadienoic acid (Z,Z) | C ₁₈ H ₃₂ O ₂ | 22.90/2.99 | |
| 7 | Ethyl linoleate | C ₂₀ H ₃₆ O ₂ | 23.43/1.72 | |
| 8 | Elcosa methyl cyclodeca siloxane | C ₄₀ H ₉₆ O ₁₂ Si ₁₀ | 27.13/0.67 | |
| 9 | Hexadecanoic acid, 2-hydroxy-1-(hydroxymethyl)ethyl ester | C ₁₉ H ₃₈ O ₄ | 28.16/2.78 | |
| 10 | Octadecanal | C ₁₈ H ₃₆ O | 28.42/0.67 | |
| 11 | Eicosane | C ₂₀ H ₄₂ | 31.07/2.50 | |
| 12 | Bis(2-ethylhexyl) phthalate | C ₂₄ H ₃₈ O ₄ | 28.69/1.43 32.04/13.66 | |
| 13 | Stigmasterol | C ₂₉ H ₄₈ O | 49.38/2.54 | |

Continued Table 1. Phytocomponents of purple Rose of Sharon flower extract by GC-MS

| Entry | Name of the Compound | Molecular Formula (MF) | RT/Peak area % | Structure |
|-------|----------------------|-----------------------------------|----------------|---|
| 14 | Gamma sitosterol | C ₂₉ H ₅₀ O | 50.80/19.72 |  |
| 15 | Alpha Amyrin | C ₃₀ H ₅₀ O | 51.25/10.43 |  |
| 16 | Aristolone | C ₁₅ H ₂₄ O | 54.24/5.21 |  |

Fig. 1. UV-Vis spectrum of biosynthesized Sm₂O₃ after 24h with the ratio of Sm(NO₃)₃: Rose of Sharon flower extract (1:1)

absorption peaks found between 300 and 500 nm were assigned to the corresponding peaks. The broad absorption below 300 nm was possibly due to the O²⁻-Sm³⁺ charge transfer [36-38]. It is well known from absorption spectroscopy that the bandgap increases by decreasing particle size. There is also an opposite ratio between bandgap and the wavelength of absorption. The absorption bands of the synthesized Sm₂O₃ nanocomposite have shown a blue shift. This optical phenomenon indicates that these nanoparticles show the quantum size effect and can be due to a high decrease in the particle size [39, 40].

The UV-Vis spectra showed that Sm₂O₃ NPs

was obtained rapidly only within the first 30 min and the Sm₂O₃ NPs in the solution remained stable even 24 hours after the completion of the reaction at room temperature.

Thermal properties of (MWCNTs)-COOH/Sm₂O₃ nanocomposite (TGA/DTA)

Differential thermal analysis (DTA) and thermal gravimetric analysis (TGA) of Sm₂O₃ NPs were carried out. From the thermal decomposition (TGA/DTA) results, several observations are worth mentioning. It was performed to estimate the final amount, and consequently the thermal behavior of the nanocomposite. It was investigated



Fig. 2. TGA and DTA curves of Sm₂O₃ NPs

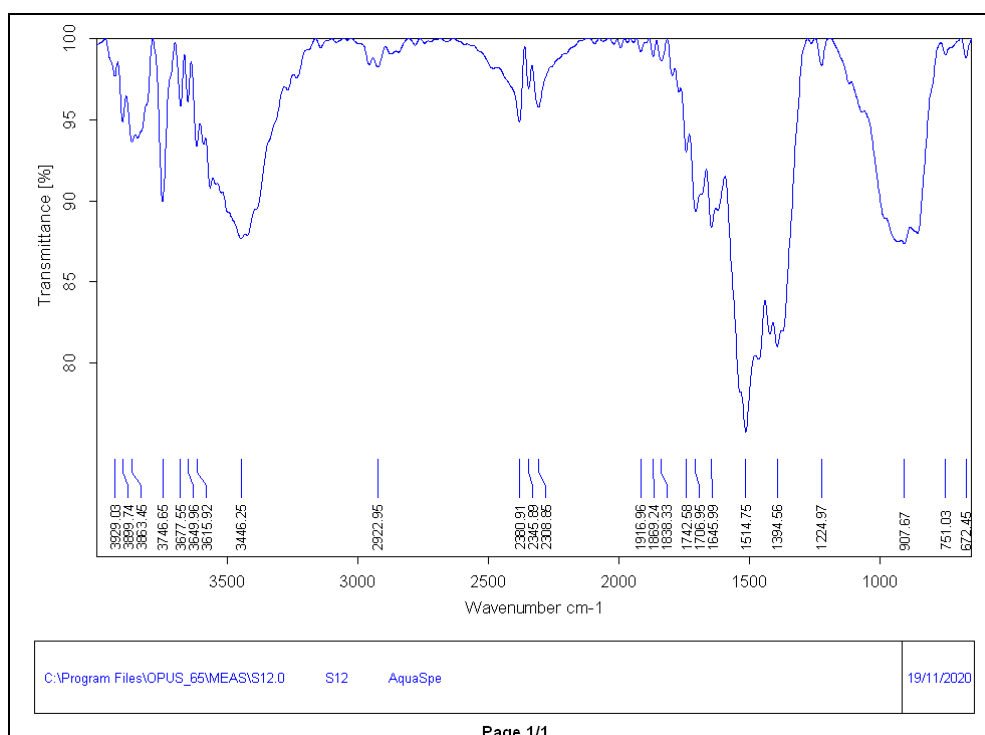
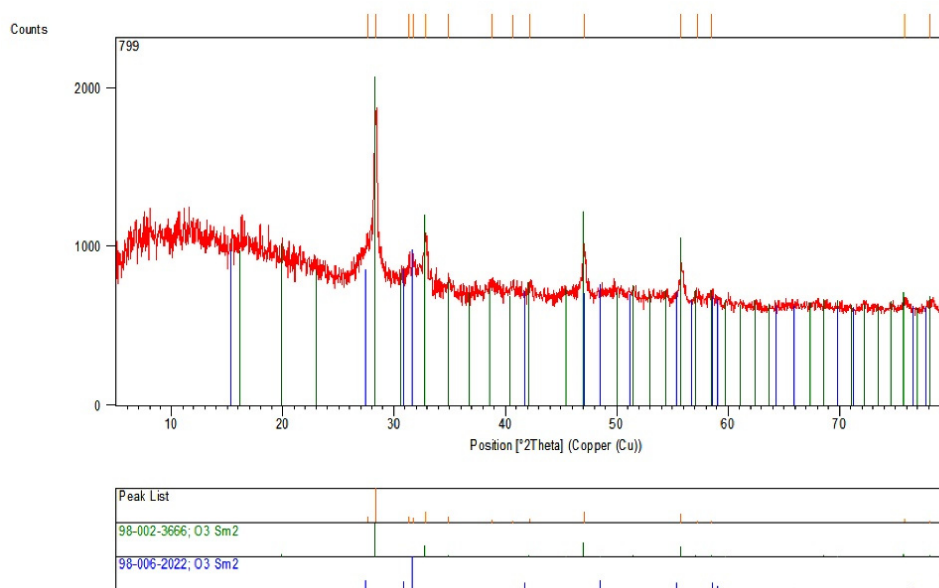
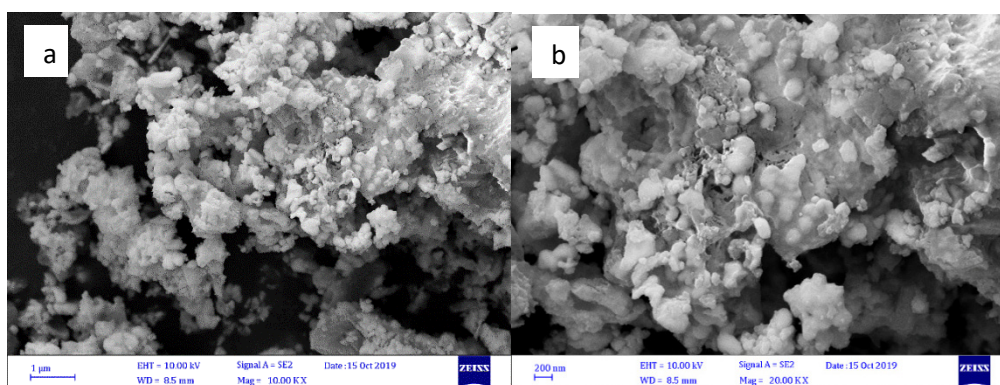


Fig. 3. FT-IR spectra of Sm₂O₃ NPs

in the temperature range of 25 to 1000 °C. Typical thermal TGA and DTA curves are given in Fig. 2. There is no weight loss in the range of 0–350 °C which indicates the absence of coordinated or uncoordinated water molecules. The exothermic DTA peak at 666 °C was recorded. After about 600°C, the samples started to present a significant mass loss. This is attributed to the decomposition of the remaining plant compounds on the surface of the nanoparticles into CO₂ by atmospheric

oxygen. The oxidation peak, observed in DTA curves, occurs at about 666°C. The final residue was analyzed as Sm₂O₃ which revealed thermal stability from 800 to 1000 °C.

The possible interaction between Sm(NO₃)₃.6H₂O and Rose of Sharon flower extract was investigated using FT-IR spectroscopy, which leads to the preparation and stabilization of Sm₂O₃ NPs. As shown in Fig. 3, typical FT-IR spectra of Sm₂O₃ NPs can be clarified briefly.

Fig. 4. XRD patterns of Sm₂O₃ NPsFig. 5. SEM image of Sm₂O₃ NPs

The results in these spectra show that the data are the same as reported in the literature [38]. The strong and broad absorption band at 600–900 cm^{-1} is related to the O–Sm-, which confirms the formation of Sm₂O₃ NPs. A broad band at 3446 cm^{-1} is attributable to the stretching vibration of –OH and H–O–H molecules absorbed physically on the surface of Sm₂O₃ NPs. The contact of trapped water in the nanoparticles with CO₂ originating from the air can result in the formation of carbonate ions characterized by a peak situated at 1514 cm^{-1} [41, 42]. The broad absorption band at around 3421 cm^{-1} is related to O–H and H–O–H molecules absorbed physically on the surface of Sm₂O₃ NPs. Following the calcinations of the hydroxide sample at 500 °C, the strong absorption bands which appear at 600-900 (652, 751, 950) cm^{-1} are related

to Sm–O stretching vibration [43]. The protein and some chemical compounds from plant extracts might play an important role in the stabilization of nanoparticles by binding to or encapsulating them. This action forms a layer around nanocomposites and protects them from agglomeration [44, 45].

The crystalline structure and average size of Sm₂O₃ nanoparticles were identified with the XRD technique. As shown in Fig. 4, the XRD pattern of Sm₂O₃ nanoparticles demonstrates high intense peaks in the whole spectrum of 2θ values ranging from 20° to 80°, which correspond to the hexagonal phase of Sm₂O₃ nanoparticles. They are consistent with the standard pattern for JCPDS Card No. (98-002-3666 and 98-006-2022) [46, 47] and confirmed that Sm₂O₃ nanoparticles had been formed. The average diameter is obtained as about

35.6 nm according to the line width analysis of the diffraction peaks based on the Debye–Scherrer equation [48] ($D = K\lambda/\beta\cos\theta$, where K is constant, β is the peak width at half maximum and λ is X-ray wavelength).

The SEM images in Fig. 5 show the morphology and particle size of Sm₂O₃. In this method, the samples were turned to hexagonal particles with much less agglomeration when calcined at high temperatures. The particles' diameter and size were measured. The size of most NPs are in the range of nanometers (around 30-70 nm).

Fig. 6 shows the transmission electron microscopy (TEM) images of the Sm₂O₃ NPs. We can see that the Sm₂O₃ NPs are composed of small particles. The average particle size is about 30-70 nm.

In Fig. 7, EDX analysis was performed to confirm the elements present in the resulting Sm₂O₃ NPs. For using SEM/EDS to analyze the

composition of a sample, usually, a heavy metal such as Au (Au-Pd) was coated with the sample to make it conductive before inserting it into FE-SEM. Therefore, there is a sign of coating metal (Au) in EDX. In addition, the analysis reveals the presence of Sm and O (Sm₂O₃ NPs) in the sample.

In the preliminary stage of the investigation, the model reaction of *o*-phenylenediamine, and D-mannose was carried out by using various amounts of NPs in various solvents and solvent-free conditions. The optimum amount of Sm₂O₃ NPs was 5 mol% as shown in Table 2. Increasing the amount of the catalyst to more than 5 mol% does not improve the yield of the product any further, whereas decreasing the amount of the catalyst leads to a decrease in the product yield (Table 2).

We found that in the absence of Sm₂O₃ NPs, the yield of the product on the TLC plate was not satisfactory even after 4h of the reaction. The best results were obtained with 5 mol% of Sm₂O₃ NPs

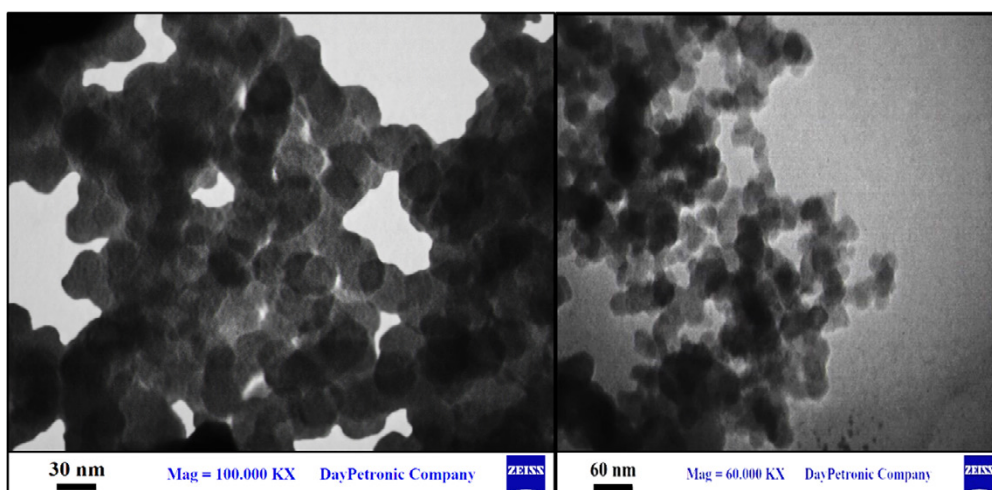


Fig. 6. TEM images of Sm₂O₃ NPs

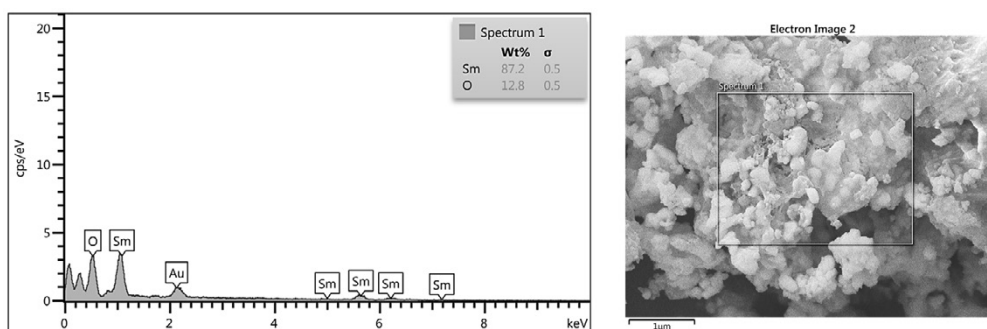


Fig. 7. Energy dispersive spectra (EDS) of Sm₂O₃ NPs

Table 2. The reaction of ortho phenylenediamine (1 mmol) and D-mannose (1 mmol) under different conditions

| Entry | Solvent | Sm ₂ O ₃ NPs (mol%) as a catalyst | Time (hours) | Yield ^a (%) |
|-------|---------------------------------|---|--------------|------------------------|
| 1 | THF | - | 4 | trace |
| 2 | THF | 3 | 4 | 45 |
| 3 | THF | 4 | 2 | 54 |
| 4 | THF | 5 | 2 | 75 |
| 5 | THF | 7 | 2 | 76 |
| 6 | H ₂ O | - | 4 | trace |
| 7 | H ₂ O | 3 | 4 | 48 |
| 8 | H ₂ O | 4 | 2 | 65 |
| 9 | H ₂ O | 5 | 2 | 72 |
| 10 | H ₂ O | 7 | 2 | 72 |
| 11 | EtOH | - | 4 | trace |
| 12 | EtOH | 3 | 4 | 43 |
| 13 | EtOH | 4 | 2 | 57 |
| 14 | EtOH | 5 | 2 | 83 |
| 15 | EtOH | 7 | 2 | 82 |
| 16 | EtOH 70% | - | 2 | trace |
| 17 | EtOH 70% | 3 | 2 | 53 |
| 18 | EtOH 70% | 4 | 2 | 69 |
| 19 | EtOH 70% | 5 | 2 | 96 |
| 20 | EtOH 70% | 7 | 2 | 97 |
| 21 | CH ₂ Cl ₂ | - | 4 | - |
| 22 | CH ₂ Cl ₂ | 3 | 4 | 31 |
| 23 | CH ₂ Cl ₂ | 4 | 2 | 37 |
| 24 | CH ₂ Cl ₂ | 5 | 2 | 48 |
| 25 | CH ₂ Cl ₂ | 7 | 2 | 48 |
| 26 | Solvent-free | - | 4 | trace |
| 27 | Solvent-free | 3 | 4 | 36 |
| 28 | Solvent-free | 4 | 2 | 46 |
| 29 | Solvent-free | 5 | 2 | 62 |
| 30 | Solvent-free | 7 | 2 | 62 |

^a Isolate Yield.

in ethanol 70% under reflux conditions (Table 2, Entry 14).

To evaluate the scope and limitations of this methodology, we extended our study to include a variety of structurally different sugars with *o*-phenylenediamine. The results are summarized in Table 3 (entries 1–6). In almost all cases, the reactions proceeded smoothly within 90–120 min, providing the corresponding products in good isolated yields.

Characterization and spectral data of the newly synthesized compounds are presented in Tables 4 and 5, respectively.

FT-IR spectra of compounds (1–6) were investigated in the frequency range of 400–4000 cm⁻¹ (Table 4). The bands at about 1602–1624 and 1438–1542 cm⁻¹ belonged to the C=N and

C=C double bonds stretching vibration of the synthesized compounds. The bands at about 1017–1402 cm⁻¹ indicated the existence of C-O and C-N groups. The ¹H NMR and ¹³C NMR spectra of all the compounds (1–6) are presented in Table 5.

The structures of compounds 1–6 are confirmed by IR, ¹H NMR, ¹³C NMR, and CHN analysis. For example, the ¹H NMR spectrum of compound 4 shows singlet at 12.30 ppm for NH proton and five doublet signals at 5.82, 4.55, 4.52, 4.36, and 4.08 ppm for OH protons. The aromatic protons were presented at 7.50 and 7.13 ppm. In the ¹³C NMR spectrum, the resonances related to carbon groups of HO-C- were appeared at 72.01, 71.61, 70.27, 68.64, and 64.29 ppm. The signals attributed to unsaturated carbon double bonds (-N=CH-) and (-CH=CH-) have appeared at

Table 3. Production of benzimidazole derivatives using Sm₂O₃ NPs in ethanol 70%

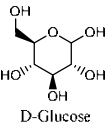
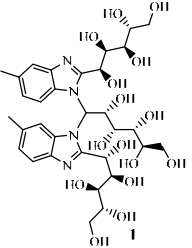
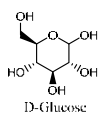
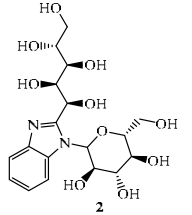
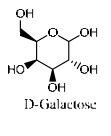
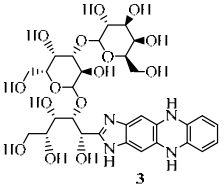
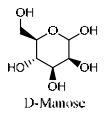
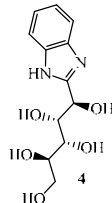
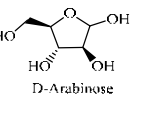
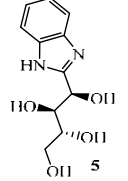
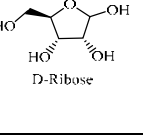
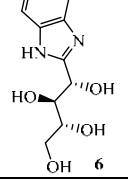
| Entry | Sugar | Product | Compounds name | Reaction time (min) in ethanol 70% | m.p °C | Yield% |
|-------|--|--|---|------------------------------------|--------|--------|
| 1 |  D-Glucose |  1 | (2R,3R,4R,5S)-6-(5-methyl-2-((1S,2R,3R,4R)-1,2,3,4,5-pentahydroxypentyl)-1H-benzo[d]imidazol-1-yl)-6-(6-methyl-2-((1S,2R,3R,4R)-1,2,3,4,5-pentahydroxypentyl)-1H-benzo[d]imidazol-1-yl)hexane-1,2,3,4,5-pentaol | 120 | >300 | 87 |
| 2 |  D-Glucose |  2 | (1S,2R,3R,4R)-1-(1-((3R,4S,5S,6R)-3,4,5-trihydroxy-6-(hydroxymethyl)tetrahydro-2H-pyran-2-yl)-1H-benzo[d]imidazol-2-yl)pentane-1,2,3,4,5-pentaol | 120 | 152 | 94 |
| 3 |  D-Galactose |  3 | (2R,3S,4R,5S)-5-(5,10-dihydro-1H-imidazo[4,5-b]phenazin-2-yl)-4-(((3R,4S,5S,6R)-3,5-dihydroxy-6-(hydroxymethyl)-4-(((3R,4S,5R,6R)-3,4,5-trihydroxy-6-(hydroxymethyl)tetrahydro-2H-pyran-2-yl)oxy)tetrahydro-2H-pyran-2-yl)oxy)pentane-1,2,3,5-tetraol | 120 | 202 | 90 |
| 4 |  D-Mannose |  4 | (1R,2R,3R,4R)-1-(1H-benzo[d]imidazol-2-yl)pentane-1,2,3,4,5-pentaol | 90 | 205 | 96 |
| 5 |  D-Arabinose |  5 | (1R,2S,3R)-1-(1H-benzo[d]imidazol-2-yl)butane-1,2,3,4-tetraol | 90 | 275 | 97 |
| 6 |  D-Ribose |  6 | (1S,2S,3R)-1-(1H-benzo[d]imidazol-2-yl)butane-1,2,3,4-tetraol | 90 | 220 | 95 |

Table 4. Characterization data for compounds (1-6)

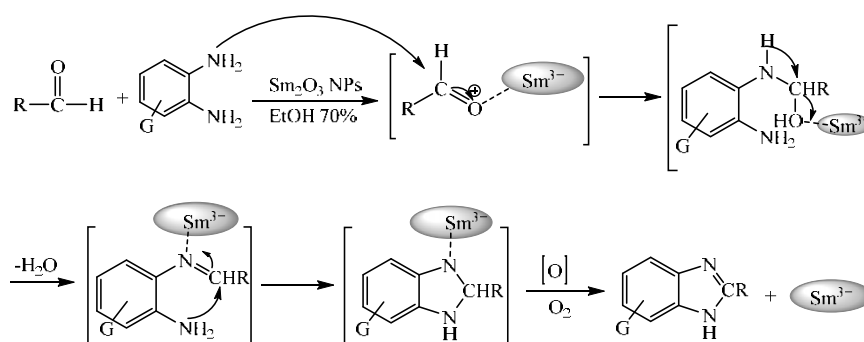
| Comp. No. | FT-IR (KBr, ν_{\max} cm^{-1}) | Mol. formula (m/z) | Elemental analysis, found (calcd.) |
|-----------|---|--|---|
| | | | C; H; N |
| 1 | 3000-3500 (OH, NH), 3371 (NH), 2923 (CH), 1625 (C=N), 1517 (C=C), 1452 (C=C), 1332 (C-N), 1229 (C-N), 1079 (C-O), 1040 (C-O) | $\text{C}_{32}\text{H}_{46}\text{N}_4\text{O}_{15}$ (726.30) | 52.93 (52.89); 6.47 (6.38); 7.66 (7.71) |
| 2 | 3000-3683 (OH), 3376 (OH), 3025 (CH_{Ar}), 2927 (CH_{Aliph}), 1604 (C=N), 1525 (C=C), 1455 (C=C), 1380 (C-N), 1319 (C-N), 1248 (C-O), 1173 (C-O), 1079 (C-O), 1017 (C-O) | $\text{C}_{18}\text{H}_{26}\text{N}_2\text{O}_{10}$ (430.16) | 50.41 (50.23); 6.13 (6.09); 6.58 (6.51) |
| 3 | 3000-3655 (OH), 3393 (OH), 3030 (CH_{Ar}), 2892 (CH_{Aliph}), 1602 (C=N), 1529 (C=C), 1510 (C=C), 1456 (C=C), 1375 (C-N), 1325 (C-N), 1247 (C-O), 1062 (C-O), 1038 (C-O) | $\text{C}_{30}\text{H}_{40}\text{N}_4\text{O}_{15}$ (696.25) | 51.65 (51.72); 5.86 (5.79); 8.12 (8.04) |
| 4 | 3324 (OH), 3020 (CH_{Ar}), 2936 (CH_{Aliph}), 1623 (C=N), 1532 (C=C), 1451 (C=C), 1402 (C-N), 1097 (C-O), 1046 (C-O), 1018 (C-O) | $\text{C}_{12}\text{H}_{16}\text{N}_2\text{O}_5$ (268.11) | 53.45 (53.73); 6.36 (6.01); 10.52 (10.44) |
| 5 | 3000-3679 (OH), 3391 (OH), 3253 (NH), 3051 (CH_{Ar}), 2925 (CH_{Aliph}), 1625 (C=N), 1537 (C=C), 1438 (C=C), 1373 (C-N), 1308 (C-N), 1271 (C-O), 1213 (C-O), 1093 (C-O), 1045 (C-O) | $\text{C}_{11}\text{H}_{14}\text{N}_2\text{O}_4$ (238.10) | 55.41 (55.46); 5.87 (5.92); 11.82 (11.76) |
| 6 | 3000-3600 (OH), 3426 (OH), 3218 (NH), 3063 (CH_{Ar}), 2924 (CH_{Aliph}), 1623 (C=N), 1542 (C=C), 1444 (C=C), 1312 (C-N), 1269 (C-O), 1215 (C-O), 1065 (C-O), 1017 (C-O) | $\text{C}_{11}\text{H}_{14}\text{N}_2\text{O}_4$ (238.10) | 55.53 (55.46); 5.97 (5.92); 11.82 (11.75) |

Table 5. NMR spectral data for compounds (1-6)

| Comp. No. | ^1H NMR (CDCl_3 (1-4), $\text{DMSO}-d_6$ (5-7), 400 MHz δ ppm) | ^{13}C NMR ($\text{DMSO}-d_6$ (5-7), CDCl_3 (1-4), 100 MHz δ ppm) |
|-----------|--|---|
| 1 | 6.68 (d, 1H, $J = 8.0$ Hz, CH_{Aro}), 6.62 (d, 1H, $J = 8.0$ Hz, CH_{Ar}), 6.13 (s, 1H, CH_{Ar}), 6.00 (d, 1H, $J = 2.0$ Hz, CH), 5.97 (dd, 1H, $J = 2.0, 8.4$ Hz, CH), 5.88 (d, 1H, $J = 2.4$ Hz, OH), 5.73 (d, 1H, $J = 2.0$ Hz, OH), 5.61 (d, 1H, $J = 7.6$ Hz, OH), 4.95 (br, 2H, OH), 4.42 (br, 2H, OH), 4.28 (m, 2H, CH), 4.23 (t, 2H, $J = 7.6$ Hz, CH_2), 3.66 (br, 1H, CH), 3.64 (m, 1H, CH), 3.46-3.38 (br, 5H, CH), 3.21 (br, 7H, CH), 3.12 (d, 5H, $J = 7.6$ Hz, CH) | 147.08, 146.59, 146.55, 145.48, 130.59, 130.49, 130.20, 111.36, 110.94, 103.53, 102.80, 100.08, 98.19, 86.22, 86.03, 85.96, 78.13, 77.94, 77.61, 77.55, 77.50, 77.19, 73.95, 73.53, 73.22, 72.79, 72.23, 71.29, 70.61, 70.52, 64.106, 61.38, 61.29, 59.49, 19.01, 17.10 |
| 2 | 6.68 (dd, 1H, $J = 3.6, 5.6$ Hz, CH_{Aro}), 6.60 (dd, 1H, $J = 3.6, 5.6$ Hz, CH_{Aro}), 5.19 (d, 1H, $J = 9.6$ Hz, OH), 4.99 (d, 1H, $J = 4.0$ Hz, OH), 4.91 (d, 2H, $J = 4.8$ Hz, OH), 4.43 (t, 1H, $J = 5.6$ Hz, OH), 4.36 (t, 2H, $J = 4.8$ Hz, OH), 4.28 (t, 1H, $J = 8.8$ Hz, OH), 3.67 (dd, 1H, $J = 5.2, 10$ Hz, CH), 3.40-3.47 (m, 5H, OH), 3.24-3.29 (m, 2H, CH), 3.21 (m, 1H, CH_2), 3.15 (m, 1H, CH) | 176.15, 168.26, 164.64, 162.01, 148.54, 141.31, 135.72, 131.45, 128.16, 122.68, 119.62, 113.70, 108.78, 104.17, 94.31, 89.06, 70.66, 56.48, 19.03 |
| 3 | 12.06 (s, 1H, NH), 7.51 (dd, 1H, $J = 2.0, 4.8$ Hz, NH), 7.44 (dd, 1H, $J = 2.0, 4.8$ Hz, NH), 7.11 (m, 2H, CH_{Aro}), 6.67 (m, 2H, CH_{Aro}), 6.59 (m, 2H, CH_{Aro}), 5.44 (d, 1H, $J = 6.8$ Hz, CH), 5.23 (d, 2H, $J = 9.6$ Hz, OH), 5.11 (dd, 2H, $J = 3.0, 7.2$ Hz, CH), 4.87 (d, 2H, $J = 3.0$ Hz, OH), 4.80 (d, 2H, $J = 5.2$ Hz, OH), 4.56 (t, 2H, $J = 4.2$ Hz, OH), 4.53 (d, 1H, $J = 7.6$ Hz, OH), 4.49 (t, 1H, $J = 6.0$ Hz, OH), 4.38 (d, 2H, $J = 3.6$ Hz, OH), 4.31 (d, 1H, $J = 8.0$ Hz, OH), 4.26 (d, 1H, $J = 4.2$ Hz, OH), 3.92 (m, 1H, CH), 3.76 (m, 1H, CH), 3.73 (t, 2H, $J = 3.6$ Hz, CH), 3.62 (m, 1H, OH), 3.55 (m, 3H, CH), 3.38-3.50 (m, 10H, CH) | 158.20, 156.35, 155.41, 148.99, 147.24, 145.97, 143.70, 140.83, 135.81, 134.40, 132.00, 131.19, 127.25, 125.64, 121.76, 119.08, 118.55, 113.46, 111.66, 92.67, 86.43, 76.10, 74.21, 70.93, 68.87, 67.89, 63.56, 61.06 |
| 4 | 12.30 (br, 1H, NH), 7.50 (br, 2H, CH_{Ar}), 7.13 (m, 2H, CH_{Ar}), 5.82 (d, 1H, $J = 5.6$ Hz, OH), 4.78 (dd, 1H, $J = 8.0, 5.6$ Hz, CH), 4.55 (d, 1H, $J = 6.4$ Hz, OH), 4.52 (d, 1H, $J = 5.6$ Hz, OH), 4.36 (t, 1H, $J = 5.6$ Hz, OH), 4.08 (t, 1H, $J = 7.2$ Hz, OH), 3.69 (br, 1H, CH_2), 3.66 (br, 1H, CH_2), 3.53 (m, 1H, CH), 3.42 (m, 1H, CH), 3.36 (m, 1H, CH) | 157.65, 143.14, 134.62, 121.66, 118.70, 111.74, 72.01, 71.61, 70.27, 68.64, 64.29 |
| 5 | 12.10 (br, 1H, NH), 7.52 (d, 1H, $J = 6.8$ Hz, CH_{Ar}), 7.44 (d, 1H, $J = 6.8$ Hz, CH_{Ar}), 7.14 (dd, 2H, $J = 3.2, 3.2$ Hz, CH_{Ar}), 5.47 (d, 1H, $J = 6.4$ Hz, OH), 5.08 (dd, 1H, $J = 1.6, 6.4$ Hz, OH), 4.70 (d, 1H, $J = 5.6$ Hz, CH), 4.63 (d, 1H, $J = 5.6$ Hz, OH), 4.40 (t, 1H, $J = 5.6$ Hz, OH), 3.77 (t, 1H, $J = 6.8$ Hz, CH_2), 3.66 (m, 1H, CH_2), 3.61 (m, 1H, CH), 3.44 (m, 1H, CH) | 157.84, 145.67, 134.48, 121.69, 121.23, 118.60, 111.72, 74.32, 71.48, 67.95, 63.94 |
| 6 | 12.11 (br, 1H, NH), 7.52 (br, 2H, CH_{Ar}), 7.12 (dd, 2H, $J = 2.8, 6.0$ Hz, CH_{Ar}), 5.78 (d, 1H, $J = 5.6$ Hz, OH), 4.99 (d, 1H, $J = 5.6$ Hz, CH), 4.97 (d, 1H, $J = 3.2$ Hz, OH), 4.81 (br, 1H, OH), 4.38 (t, 1H, $J = 5.6$ Hz, OH), 3.82 (q, 1H, $J = 5.6$ Hz, CH), 3.58 (m, 1H, CH_2), 3.52 (m, 1H, CH), 3.42 (m, 1H, CH) | 156.29, 142.85, 134.41, 121.94, 121.43, 118.63, 111.88, 75.08, 72.67, 69.42, 63.54 |

Table 6. A comparison of different catalysts for the synthesis of compound 5 in EtOH

| Entry | Catalyst | Amount of catalyst (mol%) | Time (hours) | Yield % |
|-------|--|---------------------------|--------------|---------|
| 1 | CuO | 10 | 4 | 69 |
| 2 | Fe ₃ O ₄ MNPs | 10 | 4 | 73 |
| 3 | Fe ₃ O ₄ @SiO ₂ -SO ₃ H MNPs | 7 | 3 | 65 |
| 4 | CaO NPs | 7 | 4 | 57 |
| 5 | ZnO-CaO NPs | 7 | 3 | 86 |
| 6 | Sm ₂ O ₃ NPs | 5 | 2 | 96 |

Scheme 2. A plausible mechanism for the synthesis of benzimidazole derivatives using Sm₂O₃ NPs

157.65, 143.14, 134.62, 121.66, 118.70, and 111.74, ppm, respectively. The elemental analysis result of compound 4 was satisfactory.

A plausible mechanism for the reaction is envisaged in Scheme 2. It is proposed that the carbonyl group of aldehyde (sugars) is primarily activated by NPs (Sm³⁺) followed by imine formation. This resulting imine further reacts with another NH₂ group of *o*-phenylenediamine to obtain dihydro benzimidazole derivatives which subsequently undergo aromatization under the oxidative condition in the open air to give the benzimidazole derivatives as shown in Scheme 1.

To investigate the efficiency of the Sm₂O₃ NPs, we compared some other metal oxide NPs for the synthesis of compound 4 and the results were summarized in Table 5. The metal oxide NPs were synthesized according to the previously reported procedures [49-54]. As shown in Table 6, the best catalyst for the synthesis of compound 4 is Sm₂O₃ NPs. Using this metal oxide as a catalyst offers several advantages such as excellent yields, short reaction times, simplicity of procedure, and using EtOH 70% as a green solvent in contrast with other metal oxides. Sm₂O₃ NPs as an efficient

heterogeneous catalyst was prepared by a simple operation from Rose of Sharon flower extract.

The catalyst was simply recovered by centrifugation, washed with ethanol, and dried at 80 °C for 2 h. The recovered catalyst was then added to a fresh reaction mixture under the same conditions and reused 4 times without significant loss of activity (Table 7). Further recycling of the nano catalyst led to a gradual loss of the catalyst during the recovering and washing stages.

CONCLUSIONS

In summary, Sm₂O₃ NPs was synthesized by *Hibiscus Syriacus Ardens* flower extract and synthesized nanoparticles characterized by UV-Vis spectroscopy, FT-IR, XRD, SEM, EDX, and TEM analyses. The results showed that Rose of Sharon flower extract to be an excellent agent for the synthesis of Sm₂O₃ NPs. After that, an efficient protocol for the synthesis of benzimidazole derivatives was described with the reaction of *o*-phenylenediamine and sugar using Sm₂O₃ NPs as a reusable catalyst in ethanol 70%. The reactions were carried out in short reaction times and the corresponding products were obtained in good

Table 7. Recycling of the Sm₂O₃ NPs catalyst

| Number of cycles | Yield ^a (%) |
|------------------|------------------------|
| 1 | 96 |
| 2 | 96 |
| 3 | 94 |
| 4 | 91 |

^a Isolated yield after chromatography

yields. In addition to having the general advantages attributed to the inherent property of the nanocatalyst, Sm₂O₃ NPs exhibited exceptionally high catalytic activity in green chemistry and increases reaction speed without pollution. Finally, this method is easier than other methods.

ACKNOWLEDGMENT

The authors wish to thank the University of Guilan and the Islamic Azad University of Qaemshahr Branch for their institutional support.

DISCLOSURE STATEMENT

The authors have no conflict of interest to declare.

REFERENCES

- [1] Bouzigues C, Gacoin T, Alexandrou A. Biological Applications of Rare-Earth Based Nanoparticles. *ACS Nano*. 2011;5(11):8488-505.
- [2] Heidarzadeh T, Nami N, Zareyee D. Application of (MWCNTs)-COOH/CeO₂ hybrid as an efficient catalyst for the synthesis of some nitrogen-containing organic compounds. *Inorganic and Nano-Metal Chemistry*. 2021:1-10.
- [3] Liang S, Wang H, Li Y, Qin H, Luo Z, Huang B, et al. Rare-earth based nanomaterials and their composites as electrode materials for high performance supercapacitors: a review. *Sustainable Energy & Fuels*. 2020;4(8):3825-47.
- [4] Abdoli M, Nami N, Hossaini Z. One-pot synthesis of spiro-acridine/indoline and indoline derivatives using (MWCNTs)-COOH/La₂O₃ hybrid as an effective catalyst. *Journal of Heterocyclic Chemistry*. 2021;58(2):523-33.
- [5] Song H-W, Kim N-Y, Park J-e, Ko J-H, Hickey RJ, Kim Y-H, et al. Shape-controlled syntheses of metal oxide nanoparticles by the introduction of rare-earth metals. *Nanoscale*. 2017;9(8):2732-8.
- [6] Escudero A, Becerro AI, Carrillo-Carrión C, Núñez NO, Zyuzin MV, Laguna M, et al. Rare earth based nanostructured materials: synthesis, functionalization, properties and bioimaging and biosensing applications. *Nanophotonics*. 2017;6(5):881-921.
- [7] Zhu W, Xu L, Ma J, Yang R, Chen Y. Effect of the thermodynamic properties of W/O microemulsions on samarium oxide nanoparticle size. *Journal of Colloid and Interface Science*. 2009;340(1):119-25.
- [8] Qiu J-D, Zhou W-M, Guo J, Wang R, Liang R-P. Amperometric sensor based on ferrocene-modified multiwalled carbon nanotube nanocomposites as electron mediator for the determination of glucose. *Analytical Biochemistry*. 2009;385(2):264-9.
- [9] Sone BT, Manikandan E, Gurib-Fakim A, Maaza M. Sm₂O₃ nanoparticles green synthesis via Callistemon viminalis' extract. *Journal of Alloys and Compounds*. 2015;650:357-62.
- [10] Gao J, Zhao Y, Yang W, Tian J, Guan F, Ma Y, et al. Preparation of samarium oxide nanoparticles and its catalytic activity on the esterification. *Materials Chemistry and Physics*. 2003;77(1):65-9.
- [11] Chin WC, Cheong KY, Hassan Z. Sm₂O₃ gate dielectric on Si substrate. *Materials Science in Semiconductor Processing*. 2010;13(5):303-14.
- [12] Michel CR, Martínez-Preciado AH, Parra R, Aldao CM, Ponce MA. Novel CO₂ and CO gas sensor based on nanostructured Sm₂O₃ hollow microspheres. *Sensors and Actuators B: Chemical*. 2014;202:1220-8.
- [13] Pan T, He X, Chen B, Chen H, Geng G, Luo H, et al. Development of benzimidazole derivatives to inhibit HIV-1 replication through protecting APOBEC₃G protein. *European Journal of Medicinal Chemistry*. 2015;95:500-13.
- [14] Zhao Ja, Guo Y, Hu J, Yu H, Zhi S, Zhang J. Potential anticancer activity of benzimidazole-based mono/dinuclear Zn(II) complexes towards human carcinoma cells. *Polyhedron*. 2015;102:163-72.
- [15] Salahuddin, Shaharyar M, Mazumder A. Benzimidazoles: A biologically active compounds. *Arabian Journal of Chemistry*. 2017;10:S157-S73.
- [16] Achar KCS, Hosamani KM, Seetharamareddy HR. In-vivo analgesic and anti-inflammatory activities of newly synthesized benzimidazole derivatives. *European Journal of Medicinal Chemistry*. 2010;45(5):2048-54.
- [17] Mahmood K, Hashmi W, Ismail H, Mirza B, Twamley B, Akhter Z, et al. Synthesis, DNA binding and antibacterial activity of metal(II) complexes of a benzimidazole Schiff base. *Polyhedron*. 2019;157:326-34.
- [18] Bektas H, Albay C, Sökmen BB, Aydın S, Menteşe E, Aydın G, et al. Synthesis, Antioxidant, and Antibacterial Activities of Some New 2-(3-fluorobenzyl)-1H-benzimidazole Derivatives. *Journal of Heterocyclic Chemistry*. 2018;55(10):2400-7.
- [19] Trivedi R, De SK, Gibbs RA. A convenient one-pot synthesis of 2-substituted benzimidazoles. *Journal of Molecular Catalysis A: Chemical*. 2006;245(1):8-11.

- [20] Bai Y, Lu J, Shi Z, Yang B. Synthesis of 2, 15-hexadecanedione as a precursor of muscone. *Synlett*. 2001;2001(04):0544-6.
- [21] Hossein A. Oskooie, Majid M. Heravi, Navvabeh Nami, Azadeh Nazari. Synthesis of some nitrogen heterocycles under microwave irradiation in solventless system. *Heterocyclic Communications*. 2005;11(1):101-4.
- [22] Mohanazadeh F, Nami N, Hosseini SS. Efficient Synthesis of 2-Arylamino-2-imidazolines and 2-Ami-nobenzimidazoles with Aminoiminomethanesulfonic Acid Derivatives. *Chinese Journal of Chemistry*. 2011;29(5):1055-8.
- [23] Heravi MM, Nami N, Oskooie HA, Hekmatshoar R. Synthesis of Thiazinobenzimidazole Derivatives in a Solventless System Under Microwave Irradiation. Phosphorus, Sulfur, and Silicon and the Related Elements. 2005;180(7):1605-10.
- [24] Mohamadi AR, Nami N, Norouzi B. Bio-directed synthesis of platinum nanoparticles by *Nymphaea alba* extract: fabrication of a novel non-enzymatic hydrogen peroxide sensor. *Journal of Materials Science: Materials in Electronics*. 2020;31(21):18721-31.
- [25] Rajabi HR, Deris H, Faraji HS. A Facile and Green Biosynthesis of Silver Nanostructures by Aqueous Extract of *Suaeda Acuminata* after Microwave Assisted Extraction. *Nanochemistry Research*. 2016;1(2):177-82.
- [26] Kaveh S, Norouzi B, Nami N, Mirabi A. Phytochemical synthesis of CdO nanoparticles: fabrication of electrochemical sensor for quantification of cefixime. *Journal of Materials Science: Materials in Electronics*. 2021;32(7):8932-43.
- [27] Sorbiun M, Shayegan Mehr E, Ramazani A, Mashhadi Malekzadeh A. Biosynthesis of metallic nanoparticles using plant extracts and evaluation of their antibacterial properties. *Nanochemistry Research*. 2018;3(1):1-16.
- [28] Ghotekar S. Plant extract mediated biosynthesis of Al₂O₃ nanoparticles- a review on plant parts involved, characterization and applications. *Nanochemistry Research*. 2019;4(2):163-9.
- [29] Sina A, Banafsheh N. Biosynthesis of Nano Nickel Oxide Powder Using *Malva sylvestris*; Evaluation of Electrochemical Activity for Determination of Cephalexin in Real Samples. *Russian Journal of Electrochemistry*. 2021;57(5):478-89.
- [30] Tahmasebi zade Damirchi J, Rostami Charati F, Akbari R, Daneshvar A. Green synthesis of silver nanoparticles using the aqueous extract of *Viscum album* Fruit. *Nanochemistry Research*. 2020;5(1):104-10.
- [31] Murthy HCAA. Green Silver Nanoparticles Synthesised Using Medicinal plant *Echinops* sp. Root Extract for Antimicrobial Applications. *Nanochemistry Research*. 2020;5(2):128-40.
- [32] Fallahi M, Norouzi B. Synthesis of cobalt oxide nanoparticles using *Cirsium vulgare* leaves extract and evaluation of electrocatalytic effects on oxidation of L-cysteine. *Ionics*. 2020;26(4):1951-61.
- [33] Kaveh S, Nami N, Norouzi B, Mirabi A. Biosynthesis of (MWCNTs)-COOH/CdO hybrid as an effective catalyst in the synthesis of pyrimidine-thione derivatives by water lily flower extract. *Inorganic and Nano-Metal Chemistry*. 2021;51(11):1459-70.
- [34] El Shazly JM, El Gayed SH, Kandil ZA, Yassin NA, Tawab SA, ElAlfy TS. Botanical and genetic characterization of *Hibiscus syriacus* L. cultivated in Egypt. *Journal of Applied Pharmaceutical Science*. 2018;8(12):092-103.
- [35] Wei Q, Ji X, Xu F, Li Q, Yin H. Chemical constituents from leaves of *Hibiscus syriacus* and their α -glucosidase inhibitory activities. *Zhong yao cai= Zhongyaocai= Journal of Chinese medicinal materials*. 2015;38(5):975-9.
- [36] Biswas S, Naskar H, Pradhan S, Chen Y, Wang Y, Bandyopadhyay R, et al. Sm₂O₃ nanorod-modified graphite paste electrode for trace level voltammetric determination of acetaminophen and ciprofloxacin. *New Journal of Chemistry*. 2020;44(5):1921-30.
- [37] Zhang H, Dai H, Liu Y, Deng J, Zhang L, Ji K. Surfactant-mediated PMMA-templating fabrication and characterization of three-dimensionally ordered macroporous Eu₂O₃ and Sm₂O₃ with mesoporous walls. *Materials Chemistry and Physics*. 2011;129(1):586-93.
- [38] Kang J-G, Min B-K, Sohn Y. Synthesis and characterization of Sm(OH)₃ and Sm₂O₃ nanoroll sticks. *Journal of Materials Science*. 2015;50(4):1958-64.
- [39] Ye X-R, Daraio C, Wang C, Talbot J, Jin S. Room temperature solvent-free synthesis of monodisperse magnetite nanocrystals. *Journal of nanoscience and nanotechnology*. 2006;6(3):852-6.
- [40] Guo-hua Z, Ming-fang L, Ming-li L. Differential pulse voltammetric determination of dopamine with the coexistence of ascorbic acid on boron-doped diamond surface. *Central European Journal of Chemistry*. 2007;5(4):1114-23.
- [41] Yousefi T, Mostaeidi MT, Ghasemi M, Ghadirifar A. A Simple Way to Synthesize of Samarium Oxide Nanoparticles: Characterization and Effect of pH on Morphology. *Synthesis and Reactivity in Inorganic, Metal-Organic, and Nano-Metal Chemistry*. 2016;46(1):137-42.
- [42] Rozenberg M, Loewenschuss A, Marcus Y. IR spectra and hydration of short-chain polyethyleneglycols. *Spectrochimica Acta Part A: Molecular and Biomolecular Spectroscopy*. 1998;54(12):1819-26.
- [43] Goldsmith JA, Ross SD. Factors affecting the infra-red spectra of planar anions with D_{3h} symmetry—IV The vibrational spectra of some complex carbonates in the region 4000-400 cm⁻¹. *Spectrochimica Acta Part A: Molecular Spectroscopy*. 1968;24(8):993-8.
- [44] Chandran SP, Chaudhary M, Pasricha R, Ahmad A, Sastry M. Synthesis of Gold Nanotriangles and Silver Nanoparticles Using *Aloe vera* Plant Extract. *Biotechnology Progress*. 2006;22(2):577-83.
- [45] Asadi Z, Nami N, Hosseinzadeh M. Green synthesis and characterization of Silver nanoparticles (Ag NPs) using white water Lily flower extraction species *Nymphaea Alba* of *Nymphaeaceae* family. *Iran J Organ Chem*. 2018;10:2403-8.
- [46] Bismayer U. Book Review. *Phase Transitions*. 2003;76(6):621-3.
- [47] Jiang S, Liu J, Lin C, Li X, Li Y. High-pressure x-ray diffraction and Raman spectroscopy of phase transitions in Sm₂O₃. *Journal of Applied Physics*. 2013;113(11):113502.
- [48] Warren BE. *X-ray Diffraction*: Courier Corporation; 1990.
- [49] Phiwandang K, Suphankij S, Mekprasart W, Pecharapa W. Synthesis of CuO Nanoparticles by Precipitation Method Using Different Precursors. *Energy Procedia*. 2013;34:740-5.
- [50] Rostami Z, Rouhanizadeh M, Nami N, Zareyee D. Fe₃O₄ magnetic nanoparticles (MNPs) as an effective catalyst for synthesis of indole derivatives. *Nanochemistry Research*. 2018;3(2):142-8.

- [51] Nami N, Nami N. Efficient solvent-free synthesis of amidines using nano-Fe₃O₄ encapsulated-silica particles bearing sulfonic acid. *Journal of Chemical, Biological and Physical Sciences, Section B*. 2015;5:1195-204.
- [52] Heidarzadeh T, Nami N, Zareyee D, editors. Synthesis of Indole Derivatives Using Biosynthesized ZnO-CaO Nanoparticles as an Efficient Catalyst. *Journal of Nano Research*; 2021: Trans Tech Publ.
- [53] Nami N, Tajbakhsh M, Vafakhah M. Application and comparison of the catalytic activity of Fe₃O₄ MNPs, Kaolin and Montmorillonite K10 for the synthesis of indole derivatives. *Quarterly Journal of Iranian Chemical Communication*. 2019;7(1, pp. 1-124, Serial No. 22):93-101.
- [54] Hasnidawani JN, Azlina HN, Norita H, Bonnia NN, Ratim S, Ali ES. Synthesis of ZnO Nanostructures Using Sol-Gel Method. *Procedia Chemistry*. 2016;19:211-6.